Computational Methods
for Shell and Spatial Structures
IASS-IACM 2000
M. Papadrakakis, A. Samartin and E. Oñate (Eds.)

KINEMATIC BIFURCATIONS IN THE SIMULATION OF DEPLOYABLE STRUCTURES

Praveen Kumar and Sergio Pellegrino

Department of Engineering
University of Cambridge, Cambridge CB2 1PZ, UK
e-mail: pellegrino@eng.cam.ac.uk

Key words: Bifurcations, Deployable structures, Mechanisms

Abstract. *This paper deals with the kinematic simulation of deployable structures that go through bifurcation points as they move. A series of algorithms are developed for structures that can be modelled using pin-jointed bars and that admit a single-parameter motion. These algorithms are able to detect and locate any bifurcation points that exist along the path of the structure and, at each bifurcation point, can determine all possible motions of the structure. The theory behind the various algorithms is explained and the analysis of a simple example is discussed in detail. Then, a simplified version of the particular problem that had motivated this work, the simulation of the folding and deployment of a thin membrane structure forming a solar sail, is analysed. For the particular cases that are considered it is found that the deployment process is inextensional, but a detailed study of the simulation results show that in more general cases it is likely that stretching or wrinkling will occur.*

1 Background and introduction

The work described in this paper originates from a series of difficulties that had been encountered in using standard algorithms to simulate the motion of deployable structures. A particular problem had been the folding/unfolding of a thin membrane for a solar sail; this had been shown to work fine by physical modelling [1] but could not be simulated.

The type of problem to be considered is best explained with reference to the simple two-dimensional pin-jointed structure shown in Figure 1(a). Bar 2 can be moved horizontally, either to the left or to the right, and downwards by mobilising its single finite amplitude mechanism. Denoting by m the number of independent mechanisms, $m = 1$ here. If bar 2 is moved to the right, the configuration shown in Figure 1(b) will be obtained and, continuing to mobilise the mechanism in the same direction, finally the configuration shown in Figure 1(c) is obtained. In this configuration two different types of motion are possible, hence $m = 2$. In the first motion bar 2 remains parallel to the base, Figure 1(b), whereas in the second motion bar 1 does not move while bars 2 and 3 rotate about joint 1, Figure 1(d). Note that this choice between two different motions is available only in the particular configuration of Figure 1(c): once the structure has left this special configuration its motion is again determined by a single parameter.

All configurations of a movable structure can be represented in a configuration space of suitable dimension. In this example, this space is $\Re^4$ because the positions of joints 1 and 2 can be defined by two cartesian coordinates per joint. A sequence of configuration changes of the type described above defines a *kinematic path* in this configuration space, and the special configuration of Figure 1(c) corresponds to a point of intersection of two different paths. This point is called a *kinematic bifurcation point*.

Consider the configuration shown in Figure 1(d) and rotate bars 2 and 3 until they overlap with bar 1. This configuration, $\mathbf{R}^B$, is also a bifurcation point where, again, two different motions are

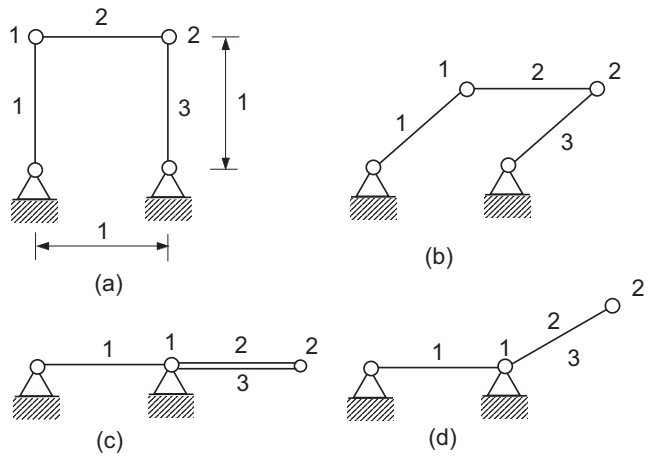

Figure 1: (a,b) Ordinary configurations of simple 2D structure; (c) kinematic bifurcation; (d) one of two possible motions out of bifurcation point.

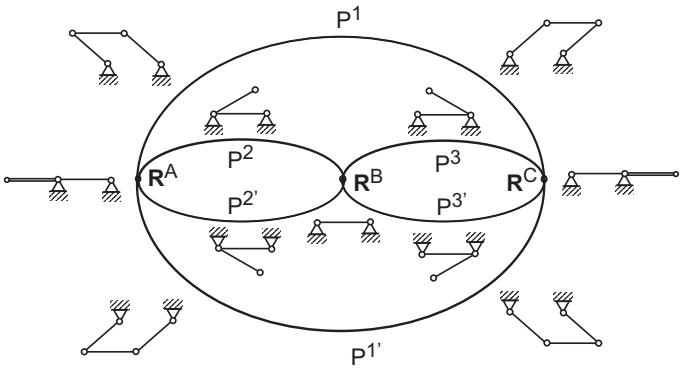

Figure 2: Topological graph showing all possible kinematic paths of structure of Figure 1.

possible. We can either rotate bars 1 and 2 about joint 2, which now coincides with the left-hand support, or rotate bars 2 and 3 about joint 1, which coincides with the right-hand support. Once one of these two options has been chosen, the structure starts following another single-parameter path.

A topological map of all existing kinematic paths for this structure is shown in Figure 2. This figure shows that there are three bifurcation points ($\mathbf{R}^B$ and $\mathbf{R}^C$ have been discussed above, while $\mathbf{R}^A$ corresponds to a configuration symmetric to $\mathbf{R}^C$) linked by three kinematic paths. The upper and lower parts of each path are labelled P^i and $P^{i\prime}$. At a bifurcation point the structure can either continue moving on a path with the same number, or it can switch to a path with a different number.

The kind of behaviour that is illustrated by the above example occurs in many structures that admit one or more finite-amplitude motions —which is indeed the case for most deployable structures— but in general obtaining a complete map like that shown in Figure 2 is by no means straightforward.

This paper presents a series of algorithms forming a computational scheme to simulate the continuous motion of a deployable structure that can be modelled using pin-jointed bars, and which admits a single-parameter motion. The scheme is able to detect bifurcation points along the path of the structure. At each bifurcation point, all possible motions of the structure can be determined, so that a particular one can be selected by the user. The layout of the paper is as follows. Section 2 gives a brief outline of the computational scheme. Section 3 presents the theory behind the various algorithms, which are divided into first-order algorithms —to simulate the motion along a uniquely determined path— and second-order algorithms —to determine all possible paths out of a kinematic bifurcation point. A solution technique for the resulting system of quadratic equations is presented. Section 4 describes the algorithm to converge to a bifurcation point. The algorithms are applied to two simple examples in Section 5, and to the deployment simulation of two small models of solar sail structures, in Section 6. Section 7 concludes the paper.

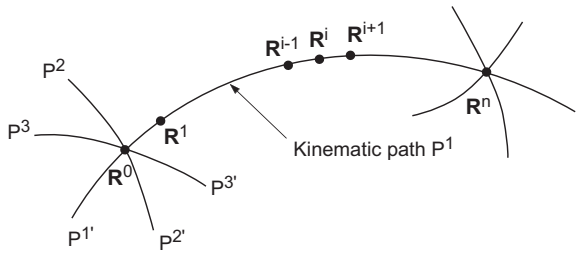

Figure 3: Kinematic path with bifurcation points at $\mathbf{R}^0$ and $\mathbf{R}^n$.

2 Outline of deployment simulation

The computations that are performed are based on the equilibrium matrix, $\mathbf{H}$, of the structure. They could also be formulated in terms of the transpose of the equilibrium matrix, i.e. the compatibility matrix. The singular value decomposition (SVD) of $\mathbf{H}$ is used to identify complete sets of independent inextensional mechanisms, from which any rigid-body mechanisms are removed, and independent states of self-stress.

If the structure is at a bifurcation point, it is necessary to determine which of its mechanisms or their combinations extend into finite motions. Although any linear combination of the set of inextensional mechanisms defines, to the first-order, a different kinematic path, only those motions that satisfy a system of second-order compatibility equations are, in fact, potential finite motions. Furthermore, it is possible that some paths actually coincide, and this can be discovered only by actually simulating finite-amplitude motions of the structure.

Once a path out of a point of bifurcation has been selected, the single internal mechanism of the structure is mobilised until the structure reaches the next bifurcation point. Along this single-parameter path, a predictor-corrector algorithm based on the SVD of the equilibrium matrix is implemented, and a special algorithm is developed to detect the existence of a bifurcation ahead of the current configuration, and to stop exactly there. Then, the analysis at the point of bifurcation is repeated.

Figure 3 shows the path followed by a structure, initially at the bifurcation point $\mathbf{R}^0$. Three different paths can be taken at $\mathbf{R}^0$, and each path has two different directions. Having chosen path P^1, a single-parameter motion is simulated until the assembly moves into another point of bifurcation, $\mathbf{R}^n$.

3 Theory

Consider a pin-jointed structure with *b* bars and *j* unconstrained joints. The equilibrium matrix $\mathbf{H}$, relating the vector of bar forces, $\mathbf{t}$, to the vector of nodal load components, $\mathbf{p}$, has dj rows —where d, which equals 2 or 3, is the dimension of the space in which the structure is being analysed— and *b* columns

$$\mathbf{Ht} = \mathbf{p} \tag{1}$$

The compatibility matrix relating the (small) nodal displacement components, **d**, to the bar extensions, **e**, is

$$\mathbf{C}\mathbf{d} = \mathbf{e} \tag{2}$$

where

$$\mathbf{C} = \mathbf{H}^T \tag{3}$$

3.1 First-order analysis

The first step in the computational procedure is the determination of the total number of independent inextensional mechanisms m and the number of states of self-stress s. These parameters can be determined from the rank r of the equilibrium matrix **H**

$$m = dj - r \tag{4}$$

$$s = b - r \tag{5}$$

In non-bifurcation configurations the structures considered in this paper have a single mechanism, $m = 1$, and no states of self-stress, $s = 0$. Hence, from Equations 4 and 5

$$dj - b = 1$$

The value of r is determined, together with orthogonal sets of m inextensional mechanisms and s states of self-stress, from the singular value decomposition (SVD) of the equilibrium matrix [2-3]. The SVD of the equilibrium matrix consists of a set of left singular vectors $\mathbf{U} = [\mathbf{u}_1, \ldots, \mathbf{u}_{dj}]$, a set of right singular vectors $\mathbf{W} = [\mathbf{w}_1, \ldots, \mathbf{w}_b]$ and a set of non-zero singular values

$$\mathbf{V} = \left[\begin{array}{c|c} \mathrm{diag}(v_1, \ldots, v_r) & 0 \\ \hline 0 & 0 \end{array}\right]$$

such that

$$\mathbf{H} = \mathbf{U}\mathbf{V}\mathbf{W}^T \tag{6}$$

The singular vectors, of unit magnitude, can be grouped into the following sub-matrices

$$\begin{array}{ll} \mathbf{U}_r = [\mathbf{u}_1, \ldots, \mathbf{u}_r], & \mathbf{U}_m = [\mathbf{u}_{r+1}, \ldots, \mathbf{u}_{r+m}] \\ \mathbf{W}_r = [\mathbf{w}_1, \ldots, \mathbf{w}_r], & \mathbf{W}_s = [\mathbf{w}_{r+1}, \ldots, \mathbf{w}_{r+s}] \end{array} \tag{7}$$

Because of the correspondence between equilibrium and compatibility matrices, Equation 3, the singular vectors have the following physical interpretation

- $\mathbf{U}_r$ contains modes of extensional deformation
  (loads that can be equilibrated by the structure, in its current configuration);
- $\mathbf{U}_m$ contains modes of inextensional deformation, or mechanisms
  (loads that cannot be equilibrated);
- $\mathbf{W}_r$ contains sets of kinematically compatible extensions corresponding, through the singular values, to the extensional modes in $\mathbf{U}_r$
  (bar forces in equilibrium with the external loads in $\mathbf{U}_r$);
- $\mathbf{W}_s$ contains sets of kinematically incompatible extensions
  (states of self-stress).

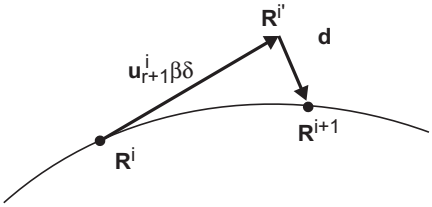

Figure 4: Predictor-corrector increments along single-parameter path.

It follows from the above that a set of bar extensions $\mathbf{e}$ is compatible if and only if it satisfies the condition

$$\mathbf{W}_s^T \mathbf{e} = 0 \tag{8}$$

Kinematic bifurcations are associated only with *internal mechanisms* and hence, if the structure admits any rigid-body mechanisms, they need to be removed from $\mathbf{U}_m$. An algorithm to remove rigid-body mechanisms from $\mathbf{U}_m$ is described in [4]; it will be assumed that $\mathbf{U}_m$ contains only internal mechanisms, m being the number of internal mechanisms.

Two different cases are possible: (i) $m = 1$ with $s = 0$, and hence in the current configuration the structure admits a single-parameter finite motion, or (ii) $m \geq 2$ with $s \geq 1$, and hence the structure is at a bifurcation point. In other words, because we are considering only assemblies with a single large displacement mechanism, if more than one infinitesimal mechanism is found in some particular configuration, then in that configuration the structure must be at a point of kinematic bifurcation.

Case (i) can be dealt with using the results of the first-order analysis described above, Section 3.2. Case (ii) requires the development of additional theory, Section 3.3, to determine the distinct kinematic paths along which the structure can move out of the bifurcation point. The computation of these kinematic paths requires the use of compatibility equations that include terms of order higher than those included in Equation 2.

3.2 Predictor-corrector incrementation

Consider a structure with $m = 1$ that is moving along a kinematic path, and assume that the current configuration, $\mathbf{R}^i$, is not a bifurcation point. To find the next configuration of the structure we impose a finite amplitude of its inextensional mechanism $\mathbf{u}_{r+1}^i$ (predictor step) and then carry out a series of iterative corrections (corrector steps) that eliminate any strain in the bars, Figure 4. The predictor step is

$$\mathbf{R}^{i'} = \mathbf{R}^i + \mathbf{u}_{r+1}^i \delta \tag{9}$$

The sign of δ controls the direction of motion. Because there is no guarantee that the SVDs of the equilibrium matrices in successive configurations will automatically produce mechanisms with consistent signs, the sign of δ has to be such that the kinematic path continues to be followed

in the desired direction. This is ensured by checking the sign of the dot product between the mechanisms in the configurations $i-1$ and i. The sign of δ is reversed if

$$\mathbf{u}_{r+1}^{i-1} \cdot \mathbf{u}_{r+1}^{i} \simeq -1 \tag{10}$$

The maximum value of δ that is allowed (smaller values may be used to increase the number of points on the path) depends upon the region of the kinematic path along which the structure is moving. If the smallest non-zero singular value, v_r, is sufficiently large the structure is far away from the next bifurcation point, and hence the magnitude of δ is chosen based upon a length parameter, such as the root mean square of all bar lengths. On the other hand, when the structure is converging towards a bifurcation point, it may be necessary to decrease the magnitude of δ, see Section 4.

In the configuration $\mathbf{R}^{i'}$ the bars of the structure have undergone extensions $\mathbf{e}$ which need to be corrected. Following References [3, 5], the minimal (in a least squares sense) correcting displacement $\mathbf{d}$ due to the extensions $-\mathbf{e}$ is computed from

$$\mathbf{d} = -\sum_{i=1}^{r} \frac{\mathbf{w}_i^T \mathbf{e}}{v_i} \mathbf{u}_i \tag{11}$$

The configuration $\mathbf{R}^{i+1} = \mathbf{R}^{i'} + \mathbf{d}$ is the strain-free configuration nearest to $\mathbf{R}^{i'}$. This corrector step can be repeated a number of times, until a desired convergence accuracy is achieved.

3.3 Second-order compatibility equations

The second-order compatibility equation for a pin-jointed bar of length L between nodes A (X_A, Y_A) and B (X_B, Y_B) has the form

$$\begin{aligned} &\frac{X_A - X_B}{L} u_A + \frac{Y_A - Y_B}{L} v_A + \frac{X_B - X_A}{L} u_B + \frac{Y_B - Y_A}{L} v_B \\ &+ \frac{1}{2L}(u_A^2 - 2u_A u_B + u_B^2 + v_A^2 - 2v_A v_B + v_B^2) = e + \frac{e^2}{2L} \end{aligned} \tag{12}$$

Introducing

$$\mathbf{d}_i = \begin{bmatrix} u_A \\ v_A \\ u_B \\ v_B \end{bmatrix}, \quad \mathbf{S} = \begin{bmatrix} 1 & 0 & -1 & 0 \\ 0 & 1 & 0 & -1 \\ -1 & 0 & 1 & 0 \\ 0 & -1 & 0 & 1 \end{bmatrix}, \text{ and } \quad e_i = e + e^2/2L \tag{13}$$

Equation 12 can be written in the form, see [6] for further details,

$$\mathbf{c}_i \mathbf{d}_i + \mathbf{d}_i^T \mathbf{S} \mathbf{d}_i = e_i \tag{14}$$

Here, e_i is a higher-order measure of the extension of bar i which, to the first-order, coincides with the standard measure (current length minus initial length); $\mathbf{c}_i$ is the the i-th row of the

compatibility matrix $\mathbf{C}$, Equation 2. For a structure with b bars we can write b equations of this type, one for each bar.

Next, consider the most general motion of nodes A and B that causes no first-order extensions in any bars of the structure. It has the expression

$$\mathbf{d}_i = \mathbf{U}_i \boldsymbol{\beta} \tag{15}$$

where the vector $\boldsymbol{\beta} = [\beta_1, \ldots, \beta_m]^T$ contains m arbitrary coefficients. $\mathbf{U}_i$ is a matrix with $2d$ rows and m columns, obtained from $\mathbf{U}_m$ by selecting the rows that correspond to bar i.

Because we are considering a motion that is first-order inextensional the first term in Equation 14 vanishes and hence the second-order compatibility equations can be written in the form

$$\boldsymbol{\beta}^T \mathbf{Q}_j \boldsymbol{\beta} = 0, \qquad j = 1, \ldots s \tag{16}$$

where

$$\mathbf{Q}_j = \sum_{i=1}^{b} t_{i,j} \mathbf{U}_i^T \mathbf{S} \mathbf{U}_i \tag{17}$$

This is a system of s quadratic equations, and hence the kinematic paths out of the point of bifurcation can be obtained by finding the intersections of the corresponding s quadric surfaces. Of the infinite number of first-order inextensional mechanisms $\mathbf{U}_m \boldsymbol{\beta}$, only those particular mechanisms that satisfy the second-order compatibility equations represent potential finite motions.

Before going further, it is convenient to normalise the quadratic forms in Equation 16. Computationally this is done by representing the matrices $\mathbf{Q}_j$ by vectors of length m^2, which are orthogonalised by the Gram-Schmidt technique [7]. Each of the resulting unit vectors is then transformed back into a square matrix $\overline{\mathbf{Q}}_j$. So, finally the system of quadratic equations is

$$\boldsymbol{\beta}^T \overline{\mathbf{Q}}_j \boldsymbol{\beta} = 0, \qquad \text{for} \quad j = 1, \ldots s \tag{18}$$

3.3.1 Solution of second-order compatibility equations

From *Bezout's Theorem* [8] the number of solutions of a system of s algebraic equations of order 2 can be at most 2^s. Consider the case $s = 3$: the $2^3 = 8$ intersection points of three ellipsoids are shown in Figure 5(a). Some, or indeed all, of these intersections may be imaginary, Figure 5(b), or there may be a smaller number of multiple intersections, Figure 5(c). Finally, there may be *improper intersections* with infinitely many points, Figure 5(d), in which case Bezout's theorem does not apply. The linear independence of the quadratic forms $\overline{\mathbf{Q}}_j$ does not give any guarantees on the type of intersection, hence all of the above cases are possible, in principle.

Solutions in closed form are possible for small values of s [6], but the most practical approach is purely numerical, using a standard non-linear equation solver. Such algorithms start from an initial starting point and perform a series of iterations to finally converge upon the nearest solution. The key to finding as many different solutions as possible lies in providing well distributed starting points spanning the entire space of first-order mechanisms. As the dimension of the

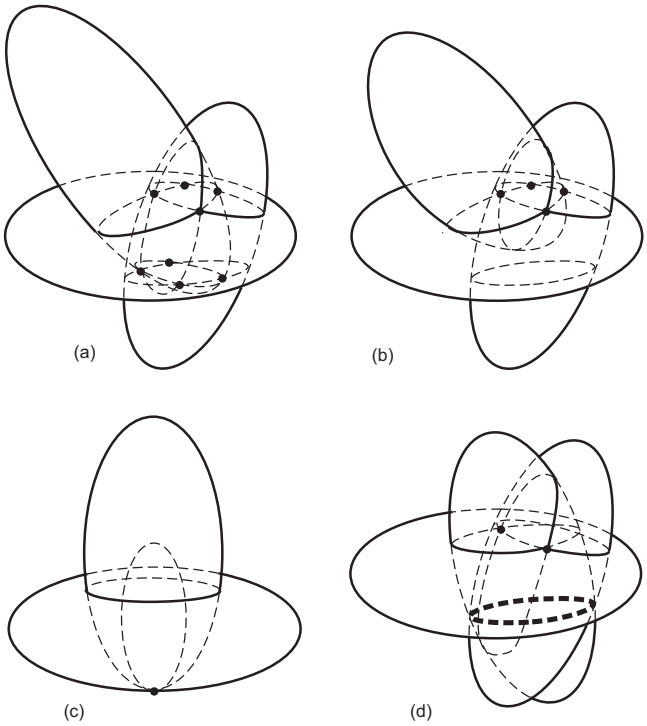

Figure 5: Intersections of three paraboloids at (a) 8 distinct points; (b) 4 distinct points; (c) 1 multiple point; (d) infinitely many points along an ellipse, plus 2 distinct points.

space is $m = s+1$, whereas there are only s equations, it is necessary to normalise the equations with respect to one variable; this introduces the normalisation condition

$$||\boldsymbol{\beta}|| = 1 \tag{19}$$

This condition represents the intersection of a hypersphere of unit radius, with the s second-order compatibility equations. For $s = 1$, for example, the space of first-order mechanisms is 2-dimensional, and this normalisation is analogous to intersecting a conic with a circle of unit radius. Similarly for $s = 2$, the space of mechanisms is 3-dimensional and we look for the intersections of 2 quadric surfaces with a unit sphere.

By considering well distributed points on this hypersphere and using them as starting points for the non-linear equation solver "fsolve" available in Matlab [9] a number of different solutions are found. Repeated solutions are eliminated by checking the dot product of each new solution with all those found previously. If the dot product is close to 1, the root has already been found. For example, if n $(< 2^s)$ solutions have been determined, then for $\boldsymbol{\beta}_{n+1}$ the dot products $\boldsymbol{\beta}_i \cdot \boldsymbol{\beta}_{n+1}$, $i = 1, \ldots, n$ are computed. If

$$|\boldsymbol{\beta}_i \cdot \boldsymbol{\beta}_{n+1}| \simeq 1 \qquad \text{for any} \quad i = 1, \ldots, n \tag{20}$$

then the root has already been found and the next starting point is considered. Otherwise, $\boldsymbol{\beta}_{n+1}$ is added to the set of solutions and n is incremented by one.

Depending on how finely the starting points are distributed on the hypersphere, an increasing proportion of the 2^s solutions will be determined.

3.4 Finite motion paths

Although each solution found in Section 3.3 defines a kinematic path out of the point of kinematic bifurcation, in fact different second-order solutions may correspond to the same kinematic path. To find out, finite-amplitude motions of the structure are considered.

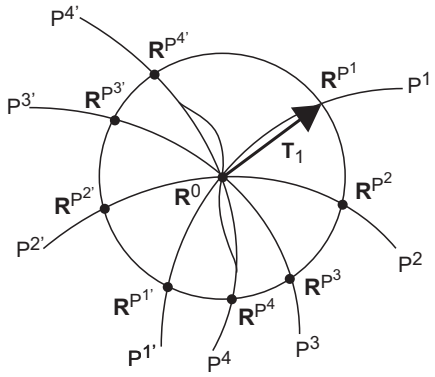

Figure 6: Identification of distinct finite motions out of a bifurcation point.

Consider a structure at the bifurcation point $\mathbf{R}^0$, Figure 6, for which a set of solutions of the second-order compatibility equations have been determined with the method of Section 3.3. Each solution defines a possible finite motion path for the structure. To test for the existence of the i-th path, we consider the finite-amplitude displacement $\mathbf{R}^0 + \mathbf{U}_m \boldsymbol{\beta}_i \delta$ and then iterate, as explained in Section 3.2, to eliminate any strain in the bars. The corrector step is repeated a number of times, until the desired convergence accuracy is achieved. If the solution does not converge after a specified number of steps, it is deemed that no finite motion path exists in the neighborhood of the i-th solution of Equation 18.

For each path that is identified, the structure is allowed to move a distance ℓ, measured along the path, using the predictor-corrector algorithm of Section 3.2. The configurations $\mathbf{R}^{Pi}$, all at distance ℓ from the point of bifurcation $\mathbf{R}^0$, are then compared. Let

$$\mathbf{T}_i = \mathbf{R}^{Pi} - \mathbf{R}^0 \tag{21}$$

To check that path i is different from the previous $i-1$ paths, the dot products of the displacement vectors are computed. If

$$\frac{|\mathbf{T}_i \cdot \mathbf{T}_j|}{||\mathbf{T}_i||||\mathbf{T}_j||} \simeq 1 \qquad \text{for any} \quad j = 1, \ldots, (i-1) \tag{22}$$

then path i has already been identified.

4 Convergence to a bifurcation point

Consider a structure that is moving along a kinematic path in a series of predictor-corrector steps with a constant step size δ, see Section 3.2. As the next bifurcation point is approached, the lowest non-zero singular value v_r starts decreasing. The kinematic simulation has to switch to a different algorithm which is capable of predicting and stopping exactly at the point of bifurcation, where a new higher-order analysis will be carried out.

Before switching to the algorithm described in this section two conditions need to be satisfied. First, v_r must be less than a certain threshold value ϵ, indicating that the assembly is getting close to a bifurcation point. Second, v_r should be decreasing in successive steps, i.e. $v_r^{n+1} - v_r^n < 0$.

As the bifurcation point is approached, a number of problems arise. First, there is the danger of numerical ill-conditioning. Second, at the bifurcation point itself, it is easy to swap paths, as a number of paths go through this point. Finally, it is possible to jump to the other side of the bifurcation without realising that this has happened.

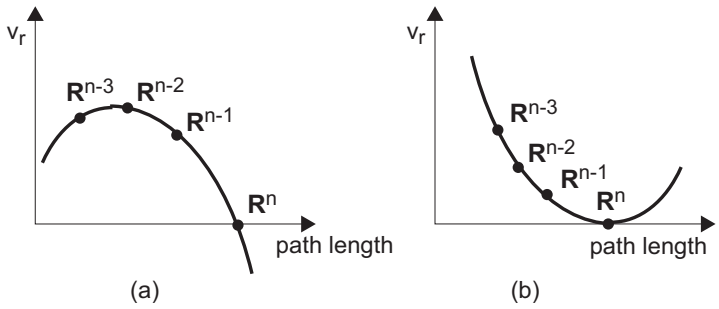

Figure 7: Variation of lowest non-zero singular value near a bifurcation point.

Consider an assembly in configuration $\mathbf{R}^{n-1}$ approaching a bifurcation point $\mathbf{R}^n$, as shown in Figure 7. To avoid the problems listed above, it is best to predict the single-step displacement to be imparted to the assembly so that it can be moved directly to $\mathbf{R}^n$. In general, the variation of the smallest singular value near a bifurcation point should be of second or higher-order. This is because each singular value relates a bar extension vector to a corresponding displacement vector [3]. Sampling v_r at the three last configurations, $\mathbf{R}^{n-3}, \mathbf{R}^{n-2}, \mathbf{R}^{n-1}$, a second-order Lagrangian polynomial in ℓ is fitted through these points

$$v_r = a\ell^2 + b\ell + c \tag{23}$$

The intersection between this polynomial and the axis $v_r = 0$ can be calculated. Depending upon the sign of the coefficient a, two cases are possible. If $a < 0$, Figure 7(a), the quadratic equation

$$a\ell^2 + b\ell + c = 0 \tag{24}$$

can be solved and, of the two solutions, the one closest to ℓ_{n-1} is chosen. If $a > 0$, Figure 7(b), the curve should be tangent to the axis $v_r = 0$, but numerical round-off causes the curve to translate

either up or down. In the former case ℓ_n is defined from the minimum of the polynomial, in the latter case it is taken to be the solution closest to l_{n-1}.

Having predicted the configuration where v_r is expected to be zero, the amplitude parameter for the step that converges to the bifurcation point is calculated from

$$\delta = \ell_n - \ell_{n-1} \tag{25}$$

Having predicted the displacement amplitude necessary to move the assembly into the point of bifurcation, a forward calculation is performed. Using the value of δ from Equation 25, the single mechanism in the configuration $\mathbf{R}^{n-1}$ is mobilised and the corresponding strain-free configuration is computed with the standard predictor-corrector algorithm. If in the new configuration $v_r = 0$, then the bifurcation has been found. Otherwise the following two checks are carried out. First, to ensure that the assembly has not switched paths, it is checked that the inextensional mechanisms in the configuration $\mathbf{R}^{n-1}$ and in the new configuration are approximately identical, hence

$$|\mathbf{u}^n_{r+1} \cdot \mathbf{u}^{n-1}_{r+1}| \simeq 1 \tag{26}$$

Second, to check that the assembly has yet to reach the bifurcation point a further, small displacement is imparted. If the smallest non-zero singular value is found to increase, it means that the assembly has already crossed the bifurcation point. If both checks are satisfied, the structure is moved from configuration $\mathbf{R}^{n-1}$ to $\mathbf{R}^n$. If either check is not satisfied, δ is decreased and the forward calculation is repeated. This iteration is repeated until v_r becomes smaller than a specified tolerance.

5 A simple example

Consider the three-bar structure of Figure 1, already discussed in Section 1. The SVD of the equilibrium matrix for the structure at the bifurcation point $\mathbf{R}^C$, Figure 1(c), is

$$\mathbf{H} = \left[\begin{array}{cc|cc} 0.7071 & 0.7071 & 0 & 0 \\ 0 & 0 & -1 & 0 \\ -0.7071 & 0.7071 & 0 & 0 \\ 0 & 0 & 0 & 1 \end{array}\right] \left[\begin{array}{ccc} 1.7321 & 0 & 0 \\ 0 & 1 & 0 \\ 0 & 0 & 0 \\ 0 & 0 & 0 \end{array}\right] \left[\begin{array}{ccc} 0.4082 & -0.8165 & -0.4082 \\ 0.7071 & 0 & 0.7071 \\ \hline 0.5774 & 0.5774 & -0.5774 \end{array}\right] \tag{27}$$

Hence, the rank of $\mathbf{H}$ is $r = 2$ and the matrices containing the $m = 2$ mechanisms and $s = 1$ states of self-stress are

$$\mathbf{U}_m = \left[\begin{array}{cc} 0 & 0 \\ -1 & 0 \\ 0 & 0 \\ 0 & 1 \end{array}\right], \qquad \mathbf{W}_s = \left[\begin{array}{c} 0.5774 \\ 0.5774 \\ -0.5774 \end{array}\right] \tag{28}$$

The coefficient matrix of the single second-order compatibility equation is computed from Equation 17

$$\mathbf{Q}_1 = 0.5774 \left[\begin{array}{cc} 0 & -1 \\ 0 & 0 \end{array}\right] \left[\begin{array}{cc} 1 & 0 \\ 0 & 1 \end{array}\right] \left[\begin{array}{cc} 0 & 0 \\ -1 & 0 \end{array}\right]$$

$$+ \quad 0.5774 \begin{bmatrix} 0 & -1 & 0 & 0 \\ 0 & 0 & 0 & 1 \end{bmatrix} \begin{bmatrix} 1 & 0 & -1 & 0 \\ 0 & 1 & 0 & -1 \\ -1 & 0 & 1 & 0 \\ 0 & -1 & 0 & 1 \end{bmatrix} \begin{bmatrix} 0 & 0 \\ -1 & 0 \\ 0 & 0 \\ 0 & 1 \end{bmatrix}$$

$$- \quad 0.5774 \begin{bmatrix} 0 & 0 \\ 0 & 1 \end{bmatrix} \begin{bmatrix} 1 & 0 \\ 0 & 1 \end{bmatrix} \begin{bmatrix} 0 & 0 \\ 0 & 1 \end{bmatrix} \tag{29}$$

This gives

$$\mathbf{Q}_1 = \begin{bmatrix} 1.1547 & 0.5774 \\ 0.5774 & 0 \end{bmatrix} \tag{30}$$

and, thus, the second-order compatibility equation is

$$[\beta_1 \beta_2] \begin{bmatrix} 1.1547 & 0.5774 \\ 0.5774 & 0 \end{bmatrix} \begin{bmatrix} \beta_1 \\ \beta_2 \end{bmatrix} = 0 \tag{31}$$

which can be simplified to

$$\beta_1^2 + \beta_1 \beta_2 = 0 \tag{32}$$

Including the normalisation condition, Equation 19, we obtain the following system of quadratic equations

$$\begin{cases} \beta_1^2 + \beta_1 \beta_2 = 0 \\ \beta_1^2 + \beta_2^2 = 1 \end{cases} \tag{33}$$

whose solutions are $\boldsymbol{\beta}_1 = [-1 \ 1]^T$ and $\boldsymbol{\beta}_2 = [0 \ 1]^T$. These two solutions correspond to two distinct kinematic paths out of $\mathbf{R}^C$, respectively shown in Figure 1(b) and 1(d).

We choose path P^1, corresponding to $\boldsymbol{\beta}_1$, and follow the motion of the structure —which has a single mechanism— until it approaches the next bifurcation point, $\mathbf{R}^A$. Convergence to this bifurcation point was achieved in a single step; the lowest non-zero singular value in the penultimate step was $v_r = 0.0052$, at this point an amplitude parameter $\delta = 0.0091$ was computed with the method of Section 4, and in the following step $v_r = 7.14 \times 10^{-7}$. Because this number is smaller than the required tolerance (10^{-6}) the structure was considered to have converged to $\mathbf{R}^A$. Hence, a new analysis of the available paths was carried out.

Figure 8 shows the variation of the lowest non-zero singular value with path length for a complete kinematic simulation starting in configuration $\mathbf{R}^A$, going to $\mathbf{R}^C$ through path P^1, then to $\mathbf{R}^B$ through path P^3, and then back to $\mathbf{R}^A$ through path P^2.

6 Folding and deployment of solar sails

An important motivation for developing the algorithms presented in this paper was being able to simulate the folding and deployment of a thin membrane structure that had been proposed by Temple and Oswald [10] for a solar powered spacecraft that would go to Mars. The original

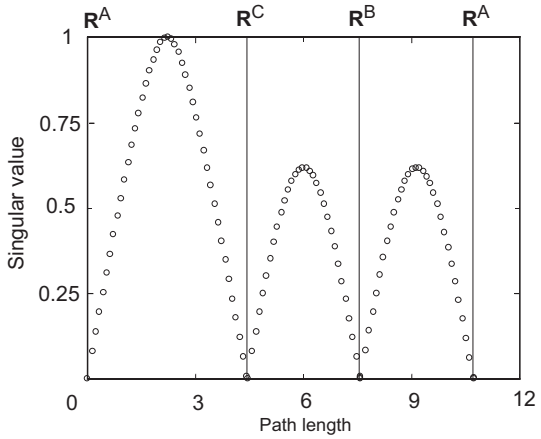

Figure 8: Variation of lowest non-zero singular value when the structure in Figure 1 moves along paths P^1, P^3, and P^2.

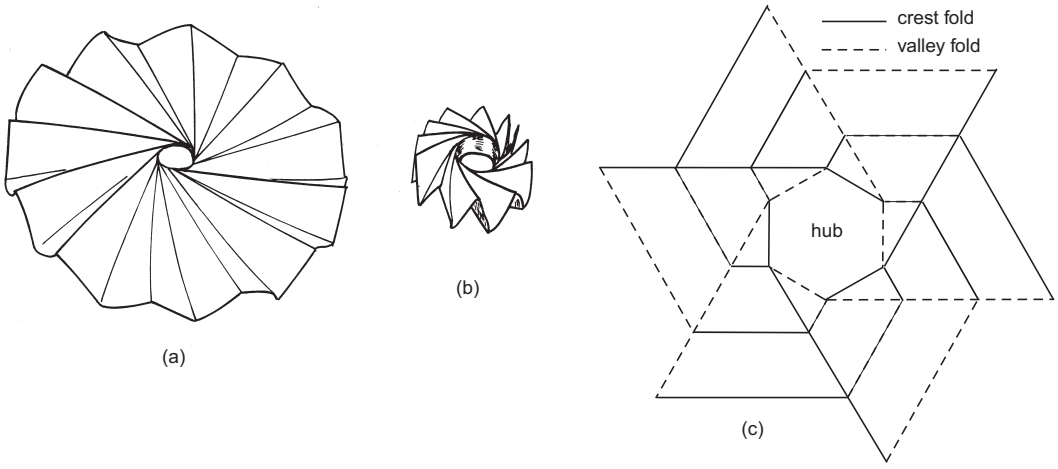

Figure 9: Wrapping of thin membrane around a central hub; (a) deployed and (b) wrapped configurations; (c) folding pattern with six near-radial folds.

proposal envisaged a circular membrane with a diameter of 276 m that, during launch, would be wrapped around a spacecraft with a diameter of 4 m.

The folding pattern that is required to wrap such a membrane around a central hub was analysed in [1]. In the simplest case this consists of an odd number of near-radial folds that crease the membrane alternately up, *valley folds*, and down, *crest folds*, intersected by sets of parallel folds. The crest and valley folds originate at the corners of a straight-sided polygon that forms the hub.

To make small physical models of this structure it is fine to assume that the membrane has zero thickness, in which case the crest and valley folds are straight. However, in larger models one has to account for the gradual increase in the effective size of the hub as the membrane is wrapped around it.

These fold patterns are worked out by considering only the fully-folded and fully-deployed configurations. Hence, they do not guarantee that the folding process itself will not require either stretching of the membrane, or changing the shape of the fold lines. The only way of finding out if small effects of this kind play a role in this type of folding is to carry out a kinematic simulation of the folding/deployment process.

Thus, the three main questions to be answered by the simulation are:

- Does there exist a continuous, strain-free motion that takes the assembly from the open to the folded configuration?
- Is there a possibility that the membrane might deploy/retract into an unexpected configuration, due to the existence of bifurcation points along its path?
- Does the hub remain planar during this motion?

To answer these questions, the membrane will be assumed to be of zero thickness, and modelled as a pin-jointed bar assembly consisting of bars placed along the fold lines of the membrane. An additional pin-jointed bar is placed along a diagonal of each trapezium bounded by successive parallel folds.

6.1 Square hub

Here we analyse a solar sail of the smallest possible size and with the smallest possible number of crest and valley folds, i.e. four in total. Its pin-jointed model is shown in Figure 10. This assembly has $b = 16$ bars and $j = 6$ non-foundation joints. Two joints, 1 and 3, are fully constrained. In a general configuration this structure has two finite inextensional mechanisms, a rigid-body rotation about the axis 1-3, and an internal mechanism.

To simulate the folding process, the equilibrium matrix of the pin-jointed assembly was set up in the fully deployed, i.e. flat, configuration. The SVD of this matrix gave six independent mechanisms and, after elimination of the rigid-body mechanism, a set of five internal mechanisms $\mathbf{U}_m$ was obtained. A set of four independent states of self-stress $\mathbf{W}_s$ was also obtained.

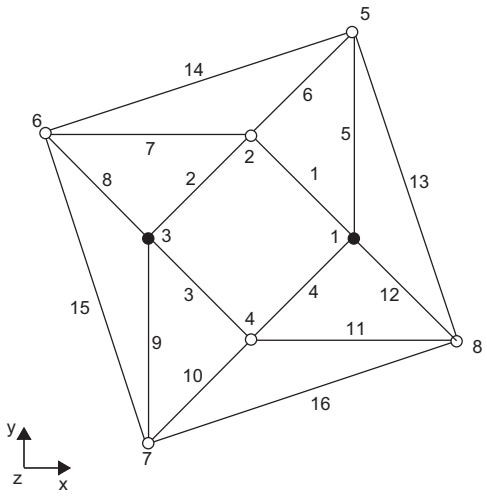

Figure 10: Pin-jointed model of smallest model of solar sail.

Since $s = 4$, from Bezout's theorem $2^4 = 16$ solutions can be expected. 15 solutions were found with the root scanning procedure: Figure 11 shows the configurations that were obtained by simulating the motion of the structure along these 15 paths. All of these configurations are at a distance $\ell = 1.75$ from the flat configuration. Note that a number of kinematic paths are related by symmetry considerations, as the assembly has four-fold cyclic symmetry and the folding pattern has two-fold symmetry. For example, path 8 can be obtained by rotating path 6, through 180° about the z-axis.

Path 12 corresponds to the path that takes the sail into its fully folded configuration. Nodes 2 and 4 move down (into the paper), whereas nodes 5 and 7 move up (out of the paper). In fact, there is a second path that also takes the sail into its fully folded configuration, corresponding to the 16th solution —which was not identified by the root scanning procedure. This alternative path requires nodes 2 and 4 to move up while nodes 5 and 7 move down. In both cases, two hub nodes have to move out of plane. Thus, depending upon the motion of the hub, up or down, two equivalent kinematic paths leading to the same compact configuration exist.

6.2 Hexagonal hub

We will now consider the folding of a pin-jointed structure that consists of two loops of triangles that wrap around a six-sided hub, Figure 12. This (slightly) more realistic model of the solar sail will allow us to give complete answers to the three questions that were posed at the beginning of this section.

Three of the hub nodes, 2, 3 and 4, are fully constrained. The other three nodes are connected by bars to node 1, which is allowed to move only in the z-direction, to maintain the hexagonal shape of the hub. The equilibrium matrix of this assembly has size 46×45. In a general configuration the assembly has only one finite internal mechanism, but in the fully deployed, flat configuration

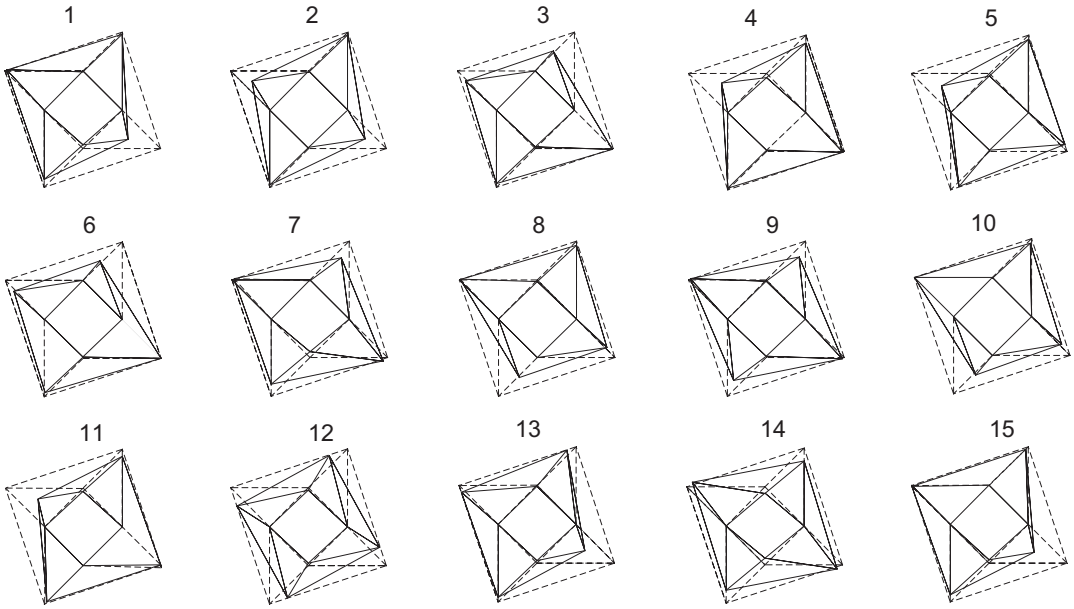

Figure 11: Projections onto x, y plane of 15 of $2^4 = 16$ motions out of fully-deployed configuration, for solar sail with square hub.

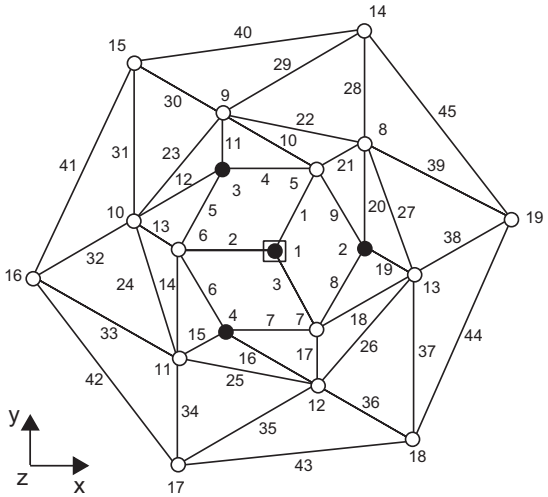

Figure 12: Pin-jointed model of small solar sail with 6 near-radial folds and hexagonal hub, cf. Figure 9(c).

$\mathbf{R}^A$ in which we started our simulation there are $m = 16$ independent infinitesimal mechanisms and $s = 15$ independent states of self-stress.

After a laborious analysis of this bifurcation point, with its potential 2^{15} paths, the correct kinematic path was picked up, thus starting the motion illustrated in Figure 13. Figure 13(c) shows a partially folded configuration where nodes 8-13 lie directly above or below the hub nodes. This configuration corresponds to the bifurcation point $\mathbf{R}^B$, which our algorithm took 35 steps to converge to. Although in this configuration the hub is planar, it distorts out-of-plane during the motion from $\mathbf{R}^A$ to $\mathbf{R}^B$. At $\mathbf{R}^B$ there are $m = 4$ infinitesimal mechanisms and $s = 3$ states of self-stress and, having computed $2^3 = 8$ distinct finite paths, it was found that there are two axi-symmetric motions both of which lead to the correct folded configuration. These two solutions correspond to node 1 moving up or down, respectively.

As the assembly approached the fully folded configuration $\mathbf{R}^C$, three non-zero singular values started approaching zero. The configuration $\mathbf{R}^C$, shown in Figure 13(e), is also a bifurcation point, which took 26 steps to converge to. In this configuration the central hub is again planar.

Next, the structure was deployed back to the original configuration $\mathbf{R}^A$. The deployment simulation began with an analysis of bifurcation point $\mathbf{R}^C$, where an axisymmetric deployment path was chosen. During deployment the assembly passed through the bifurcation point $\mathbf{R}^B$ and, finally, as it approached the fully open configuration, 15 singular values started approaching zero. Convergence to the bifurcation point $\mathbf{R}^A$ required 149 simulation steps.

The variation of the 15 singular values that were zero at the start of the simulation described above are plotted in Figure 14 for the entire kinematic simulation. One singular value is always zero, corresponding to the single internal mechanism. Due to the cyclic symmetry of the assembly, some of the singular values coincide and therefore the number of distinct curves that are visible on the plot is actually less than 15.

Note that the plot in Figure 14 is symmetric about the centre line, as the same path was followed both during folding and deployment. In fact, it is possible to change path at the first bifurcation and follow an alternative path. This would also produce the correct folding pattern, but the variation of the singular values would no longer be symmetric.

Also note that the number of steps taken to converge to successive bifurcation points increased during the course of the simulation. Thus, it took 35, 26, 58 and 149 steps to converge to the bifurcation points $\mathbf{R}^B$, $\mathbf{R}^C$, $\mathbf{R}^B$ and $\mathbf{R}^A$, respectively. It appears that there is a link between the rank deficiency of the equilibrium matrix, i.e. the number of singular values that are approaching zero, and the number of iteration steps required for convergence. However, the build up of numerical errors and inaccuracies may also be a significant effect, since convergence to the same configuration, $\mathbf{R}^B$, required 35 steps the first time and 58 the second time.

7 Discussion

The kinematic simulations described in Section 6 suggest that the deployment/folding behaviour of a theoretical membrane of zero thickness and with straight folds is *strictly inextensional*, if the

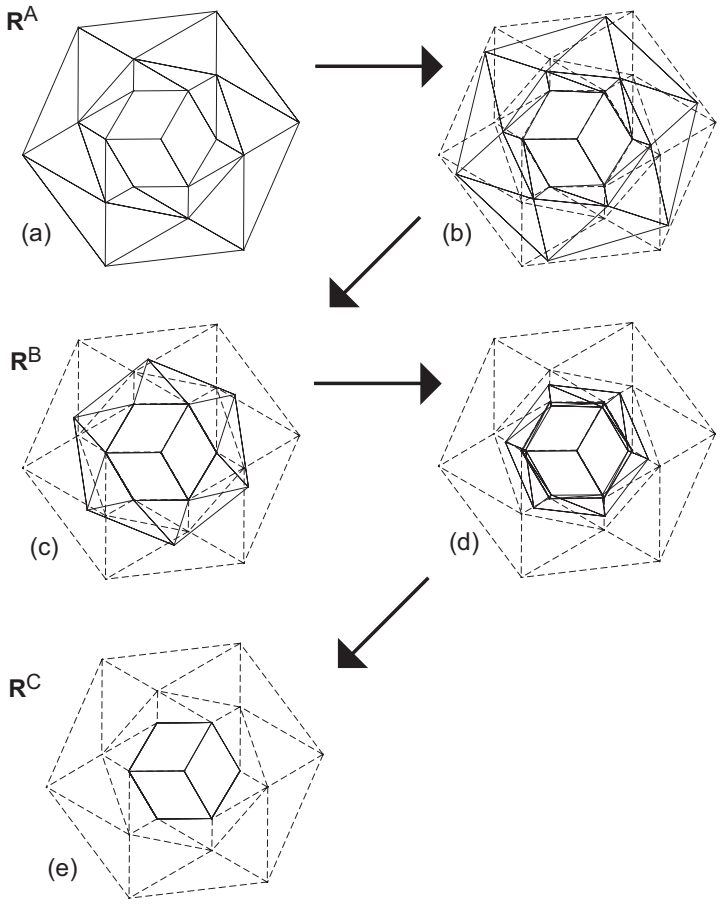

Figure 13: Projection onto x, y plane of folding simulation of structure in Figure 12.

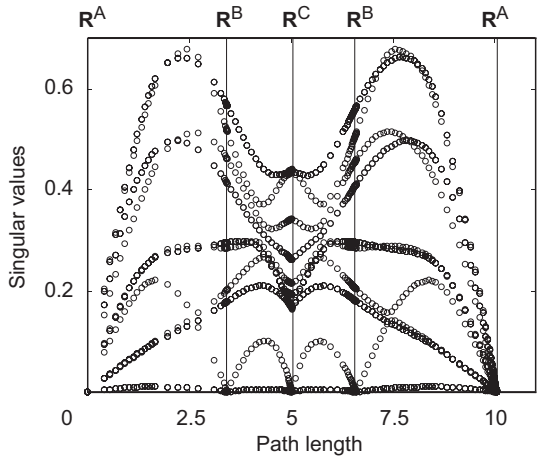

Figure 14: Variation of 15 lowest non-zero singular values during folding and deployment of solar sail model of Figure 12.

hub is allowed to distort out of plane. It has been shown that the deployment process is radially sequential, i.e. a complete loop of triangles has to unwrap completely before the next loop starts unwrapping, and there is a kinematic bifurcation every time a loop completes its unwrapping.

It should be noted that in the simulation the bars and joints of the pin-jointed model of the solar sail were allowed to pass through each other, although this never happened. The part of the membrane that is already wrapped around the hub does not remain stationary, but moves by a small amount, see Figure 14(d). It can be concluded that, although in the particular simulations that we have carried out there was no physically unacceptable interference between different parts of the membrane, it is likely that there would be interference if one considered a larger solar sail, whose folding pattern consists of several loops of triangles. Of course, the effect of modelling the thickness of the membrane will also need to be considered.

References

[1] S. D. Guest, S. Pellegrino, *Inextensional wrapping of flat membranes*, In R. Motro, T. Wester (eds) *Proc. First International Seminar on Structural Morphology*, LMGC, Universite Montpellier II, Montpellier,(1992) 203-215.

[2] G.H. Golub, C.F. van Loan, *Matrix Computations*. North Oxford Academic Publishing Co., Oxford, (1983).

[3] S. Pellegrino, *Structural computations with the SVD of the equilibrium matrix*, Int. J. Solids Structures, 30, (1993), 3025-3035.

[4] S. Pellegrino, C.R. Calladine, *Matrix analysis of statically and kinematically indeterminate frameworks*, Int. J. Solids Structures, 22, (1986), 409-428.

[5] J.F. Besseling, L.J. Ernst, K. Van der Werff, A.U. de Koning, E. Riks, *Geometrical and physical non-linearities: Some developments in the Netherlands*, Computer Methods Appl. Mech. Engg, 17/18, (1979), 131-157.

[6] P. Kumar, S. Pellegrino, *Computation of kinematic paths and bifurcation points*, to appear in Int. J. Solids Structures (2000).

[7] G. Strang, *Linear Algebra and its Applications,* 2nd Edn. Academic Press, New York, (1980).

[8] J.G. Semple, L. Roth, *Introduction to Algebraic Geometry*. Clarendon Press, Oxford, (1949).

[9] The Mathworks, *Matlab Version 5: User's Guide*. The Math Works, Inc. Natick, MA, (1997).

[10] Cambridge Consultants, *Design Study for a Mars Sailcraft*, Q7844/JPA/Issue 1, Cambridge Consultants Ltd,(1989).